NASA CONTRACTOR REPORT

NASA CR-2060

BOUNDARY LAYER STABILITY ON A YAWED SPINNING BODY OF REVOLUTION AND ITS EFFECT ON THE MAGNUS FORCE AND MOMENT

by I. D. Jacobson and J. B. Morton

Prepared by
UNIVERSITY OF VIRGINIA
Charlottesville, Va. 22901
for Langley Research Center

NATIONAL AERONAUTICS AND SPACE ADMINISTRATION • WASHINGTON, D. C. • JUNE 1972

1. Report No.	2. Government Accession No.	3. Recipient's Catalog No.
NASA CR-2060		

4. Title and Subtitle	5. Report Date
BOUNDARY LAYER STABILITY ON A YAWED SPINNING BODY OF REVOLUTION AND ITS EFFECT ON THE MAGNUS FORCE AND MOMENT	June 1972
	6. Performing Organization Code
7. Author(s)	8. Performing Organization Report No.
I. D. Jacobson and J. B. Morton	AEEP-4089-101-71U
9. Performing Organization Name and Address	10. Work Unit No.
Research Laboratories for the Engineering Sciences University of Virginia Charlottesville, Virginia 22901	136-13-01-16
	11. Contract or Grant No.
	NGR 47-005-149
12. Sponsoring Agency Name and Address	13. Type of Report and Period Covered
National Aeronautics and Space Administration Washington, D. C. 20546	Contractor Report
	14. Sponsoring Agency Code

15. Supplementary Notes

16. Abstract

This paper establishes the parameters important to the stability of a boundary layer flow over a yawed spinning cylinder in a uniform stream. It is shown that transition occurs asymmetrically in general and this asymmetry can be important for the prediction of aerodynamic forces and moments (e.g., the Magnus effect). Instability of the steady-state boundary layer flow is determined using "small" disturbance theory. Although this approach is strictly valid only for the calculation of the conditions for "stability in the small", experimental data indicate that in many problems, it provides a good estimate for the transition to turbulence.

17. Key Words (Suggested by Author(s))	18. Distribution Statement
Magnus effect Boundary layer Spinning body	Unclassified - Unlimited

19. Security Classif. (of this report)	20. Security Classif. (of this page)	21. No. of Pages	22. Price*
Unclassified	Unclassified	34	$3.00

*For sale by the National Technical Information Service, Springfield, Virginia 22151

I. INTRODUCTION

This paper establishes the parameters important to the stability of a boundary layer flow over a yawed spinning cylinder in a uniform stream. It will be shown that transition occurs asymmetrically in general and this asymmetry can be important for the prediction of aerodynamic forces and moments (e.g., the Magnus effect). Instability of the steady-state boundary layer flow is determined using "small" disturbance theory. Although this approach is strictly valid only for the calculation of the conditions for "stability in the small", experimental data indicate that in many problems, it is useful in the prediction of transition to turbulence.

The stability of the boundary layer with respect to "small" disturbances has been investigated by many authors, perhaps most notable among them, Orr,[1] Sommerfeld,[2] Tollmien,[3] Schlichting,[4] Lin,[5] and Squire.[6] The basis for the present work can be traced primarily to the work of Lin, Squire, and Kuethe.[7]

There has been little experimental data generated on the boundary layer properties of spinning bodies at small angles of attack. Thorman[8] investigated experimentally the boundary layer on an ogive cylinder but did not make sufficient measurements to map the transition line. Furuya, Nakamura and Kawachi[9] measured the momentum thickness on a spinning body of revolution, which was unyawed, for various values of spin rate. Their data, however, are not useful here, since the body was in close proximity to the wall of the wind tunnel and hence a pressure gradient was present. It is interesting to note that their results do agree qualitatively with those presented here.

2. EQUATIONS OF MOTION - STEADY-STATE ANALYSIS

Consider a semi-infinite rotating circular cylinder of radius, R, with angular velocity, ω, situated in a parallel, incompressible flow, with free stream velocity, V_∞, at an angle-of-attack, α. The coordinate system used is fixed to the body but does not rotate with it. The origin is located at the leading edge of the cylinder, x increases in the direction of the flow, y normal to the body and z in the azimuthal direction. For the boundary layer flow the curvature of the body will be neglected,* as well as the pressure gradient in the x direction. The steady state boundary layer equations of motion[10] for this body fixed system (shown in Figure 1) are

$$u \frac{\partial u}{\partial x} + v \frac{\partial u}{\partial y} + w \frac{\partial u}{\partial z} = \nu \frac{\partial^2 u}{\partial y^2} \tag{2.1}$$

$$u \frac{\partial w}{\partial x} + v \frac{\partial w}{\partial y} + w \frac{\partial w}{\partial z} = - \frac{1}{\rho} \frac{\partial p}{\partial z} + \nu \frac{\partial^2 w}{\partial y^2} \tag{2.2}$$

$$\frac{\partial u}{\partial x} + \frac{\partial v}{\partial y} + \frac{\partial w}{\partial z} = 0 \tag{2.3}$$

where u, v, and w are the velocity components in the x, y, and z directions respectively, p the static pressure, and, ρ the density.

The radius of curvature of the body can be neglected when it, and the length from the leading edge of the body, are large compared to the boundary layer thickness. Away from the leading edge and for large

---

*As Lin[5] points out, the primary effect of curvature on a convex surface (which is the case here) is to modify the pressure gradient. In the equations themselves, an error $O(\delta/R)$ is introduced which shall be neglected.

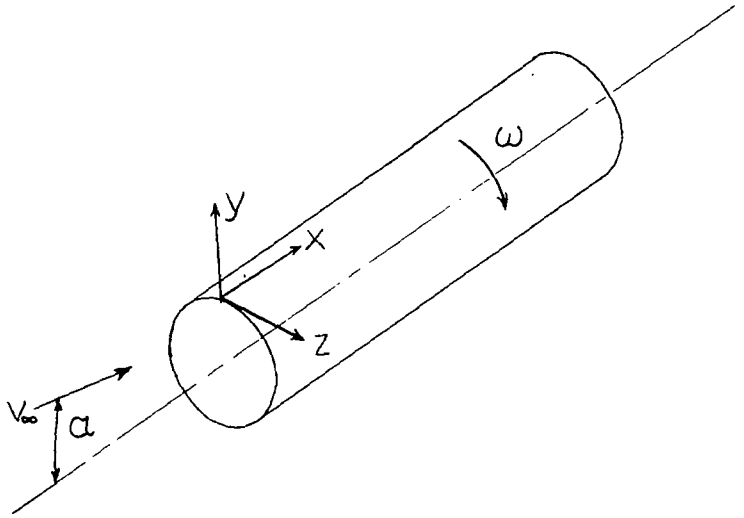

Figure 1 Coordinate System

Reynolds numbers both of these assumptions are satisfied.

There are three important nondimensional groups of parameters for this flow, the first group is the Reynolds number based on free stream velocity, V_∞, and L, where L is the distance from the leading edge.

$$R_{e_L} = \frac{V_\infty L}{\nu} . \tag{2.4}$$

The second and third groupings are

$$\omega^* = \frac{V_\infty}{\omega L} \tag{2.5}$$

and

$$\alpha^* = \frac{\alpha L}{R} \tag{2.6}$$

where ω^* will be called the reduced Rossby number (the Rossby number being the ratio $V_\infty/\omega R$; and, α^* will be called the modified angle-of-attack.

The boundary conditions for these equations are given by slender body theory as

$$u(0) = v(0) = 0 \qquad w(0) = \omega R$$

$$u(y/\delta) \to V_\infty(1 - \frac{\alpha^2}{2}) \qquad v(y/\delta) \to 0 \quad w(y/\delta) \to 2V_\infty \alpha \sin(\frac{z}{R}) \text{ as } y/\delta \to \infty$$

The pressure gradient, P_z, is that of the external potential flow, and is for small angles-of-attack,

$$P_z = -\frac{4\rho\alpha^2 V_\infty^2}{R} \sin(\frac{z}{R}) \cos(\frac{z}{R}). \qquad (2.7)$$

Using this function, equations (2.1) - (2.3) can be solved for the velocity field. It is this case that is treated in the literature and for which the solutions will be given below.

2.1 Solution

Equations (2.1) - (2.3) have been solved by Martin[10] by writing u, v, and w as perturbation series in the quantities α and $\omega R/V$, both being small for most applications. This formulation leads to the following solutions in terms of the nondimensional parameters

$$\frac{u}{V_\infty} = f_0'(\eta) + 2\alpha_\ell^* f_1(\eta)\cos(\frac{z}{R}) + \frac{\alpha_\ell^*}{\omega_\ell^*} f_2(\eta)\sin(\frac{z}{R}) + \alpha_\ell^{*2}[f_3(\eta) + f_4(\eta)\cos(\frac{2z}{R})] + \ldots \qquad (2.8)$$

$$\frac{v}{V_\infty} = \{\frac{1}{2}[\eta f_0'(\eta) - f_0(\eta)] + \alpha_\ell^* g_0(\eta)\cos(\frac{z}{R}) + \frac{\alpha_\ell^*}{\omega_\ell^*} g_1(\eta)\sin\frac{z}{R} + \ldots\} - \sqrt{\frac{\nu}{V_\infty x}} \qquad (2.9)$$

$$\frac{w}{\omega R} = 1 - (1 - 2\alpha_\ell^*\omega_\ell^*\sin(\frac{z}{R}))f_0'(\eta) + \alpha_\ell^* h_0(\eta)\cos(\frac{z}{R}) + \ldots \qquad (2.10)$$

where

$$\alpha_\ell^* = \frac{\alpha x}{R}, \quad \frac{1}{\omega_\ell^*} = \frac{\omega x}{V_\infty} \quad \text{and} \quad \eta = \frac{y}{x}\sqrt{\frac{V_\infty x}{\nu}}$$

is the Blasius similarity variable. A tabulation of the functions appearing in equations (2.8), (2.9) and (2.10) can be found in reference 10. Here '

denotes differentiation with respect to η. It is clear that the criteria for neglecting higher order terms are both α_ℓ^* and $\frac{1}{\omega_\ell^*}$ be small (i.e., $<< 1$), since all other values in the above equations are bounded by one. The consequences of this are more stringent than those imposed by the requirement that α and $\omega R/V_\infty$ be small.

3. STABILITY ANALYSIS

For the purpose of the stability analysis only terms of first order in α_ℓ^* are retained* in the steady-state solution, which becomes

$$\frac{U}{V_\infty} = f_0'(\eta) + 2\alpha_\ell^* f_1(\eta)\cos(\tfrac{z}{R}) + \frac{\alpha_\ell^*}{\omega_\ell^*} f_2(\eta)\sin(\tfrac{z}{R}) \tag{3.1}$$

$$\frac{W}{V_\infty} = \frac{\omega R}{V_\infty} + (2\alpha\sin\tfrac{z}{R}) - \frac{\omega R}{V_\infty} f_0'(\eta) + \alpha_\ell^* \frac{\omega R}{V_\infty} h_0(\eta)\cos(\tfrac{z}{R}) \tag{3.2}$$

where U and W represent the steady-state laminar boundary layer velocity profiles on the cylinder ($\frac{V}{V_\infty}$, being $O(R_{\theta_L}^{-1/2})$, will be neglected).

3.1 Equations of Motion

The Navier-Stokes equations, including time rates of change,† and, nondimensionalizing velocities on free stream velocity, V_∞, coordinates on boundary layer displacement thickness, δ, pressure on ρV_∞^2, and time on δ/V_∞ become

$$\hat{u}_{\hat{t}} + \hat{u}\hat{u}_{\hat{x}} + \hat{v}\hat{u}_{\hat{y}} + \hat{w}\hat{u}_{\hat{z}} = \frac{1}{R_{e_\delta}}(\hat{u}_{\hat{x}\hat{x}} + \hat{u}_{\hat{y}\hat{y}} + \hat{u}_{\hat{z}\hat{z}}) - \hat{P}_{\hat{x}} \tag{3.3}$$

$$\hat{v}_{\hat{t}} + \hat{u}\hat{v}_{\hat{x}} + \hat{v}\hat{v}_{\hat{y}} + \hat{w}\hat{v}_{\hat{z}} = \frac{1}{R_{e_\delta}}(\hat{v}_{\hat{x}\hat{x}} + \hat{v}_{\hat{y}\hat{y}} + \hat{v}_{\hat{z}\hat{z}}) - \hat{P}_{\hat{y}} \tag{3.4}$$

$$\hat{w}_{\hat{t}} + \hat{u}\hat{w}_{\hat{x}} + \hat{v}\hat{w}_{\hat{y}} + \hat{w}\hat{w}_{\hat{z}} = \frac{1}{R_{e_\delta}}(\hat{w}_{\hat{x}\hat{x}} + \hat{w}_{\hat{y}\hat{y}} + \hat{w}_{\hat{z}\hat{z}}) - \hat{P}_{\hat{z}} \tag{3.5}$$

$$\hat{u}_{\hat{x}} + \hat{v}_{\hat{y}} + \hat{w}_{\hat{z}} = 0 \tag{3.6}$$

---

*Terms involving $\frac{\alpha_\ell^*}{\omega_\ell^{*n}}$ $(n \geq 2)$ have also been neglected.

†Where curvature has been neglected.

where the circumflex designates the nondimensional value of the variable.

3.2 Zero Angle-of-Attack

First consider the case of zero angle-of-attack. In this case

$$\hat{u} = \frac{U_o}{V_\infty} + u^*; \quad \hat{v} = v^* \tag{3.7a, b}$$

$$\hat{w} = \frac{W_o}{V_\infty} + w^*; \quad \hat{p} = \frac{P_o}{\rho V_\infty^2} + p^* \tag{3.7c, d}$$

where U_o and W_o are the steady-state solutions (equations 3.1 and 3.2 with $\alpha_\ell^* = 0$), and the asterisked quantities denote the perturbations which have the form of a three dimensional disturbance

$$u^* = \underline{u}(\hat{y})e^{i(\gamma\hat{x} + \beta\hat{z} - c\hat{t})} \tag{3.8a}$$

$$v^* = \underline{v}(\hat{y})e^{i(\gamma\hat{x} + \beta\hat{z} - c\hat{t})} \tag{3.8b}$$

$$w^* = \underline{w}(\hat{y})e^{i(\gamma\hat{x} + \beta\hat{z} - c\hat{t})} \tag{3.8c}$$

$$p^* = \underline{p}(\hat{y})e^{i(\gamma\hat{x} + \beta\hat{z} - c\hat{t})} \tag{3.8d}$$

Here γ and β are assumed real and c complex.

The velocities and pressure are considered as the sum of a steady-state component and a perturbation. The perturbation assumed is periodic in the spatial variables $\hat{x}$, and $\hat{z}$, time $\hat{t}$, and functionally depends on the distance normal to the body $\hat{y}$. This type of disturbance is seen in

the excellent photograph by Brown[11] in which the disturbance on a spinning body at zero angle-of-attack closely resembles the classic Tollmein-Schlichting waves normal to the relative velocity vector due to both the circumferential and free stream velocities. Substituting equations (3.7), (3.8), and U_o and W_o gotten from equations (3.1) and (3.2) into equations (3.3) - (3.6) yields

$$\underline{v}'''' - 2\alpha_1^2\underline{v}'' + \alpha_1^4\underline{v} = iR_{e_\delta}\gamma[(Q_1 - C_1)(\underline{v}'' - \alpha_1^2\underline{v}) - Q_1''\underline{v}] \qquad (3.9)$$

where the primes denote differentiation with respect to $\hat{y}$, $\alpha_1^2 = \gamma^2 + \beta^2$, $Q_1 = U_o/V_\infty + \beta W_o/\gamma V_\infty$, and $C_1 = c/\gamma$. The boundary conditions are

$$\underline{v}(0) = \underline{v}'(0) = 0 \qquad \underline{v}' \sim e^{-\alpha_1 \hat{y}} \text{ for } \hat{y} \geq 1 \qquad (3.10)$$

and

$$Q_1(0) = \frac{\beta}{\gamma}\frac{\omega R}{V_\infty} \qquad Q_1(1) = 1.0 \qquad (3.11)$$

This boundary value problem has been treated in the literature, with the exception of the boundary conditions on Q_1. Equation (3.9) is transformed into that solved by Lin[5] by utilizing the following relationships; similar to those used by Kuethe[7]

$$\bar{Q} = \frac{Q_1 - \frac{\beta}{\gamma}\frac{\omega R}{V_\infty}}{1 - \frac{\beta}{\gamma}\frac{\omega R}{V_\infty}} \qquad (3.12a)$$

$$\bar{C}_1 = \frac{C_1 - \frac{\beta}{\gamma}\frac{\omega R}{V_\infty}}{1 - \frac{\beta}{\gamma}\frac{\omega R}{V_\infty}} \tag{3.12b}$$

$$\bar{R}_{e_\delta} = \frac{\gamma}{\alpha_1}\left(1 - \frac{\beta}{\gamma}\frac{\omega R}{V_\infty}\right)R_{e_\delta} \tag{3.12c}$$

Substituting equations (3.12) into (3.9) yields

$$\underline{v}'''' - 2\alpha_1^2\underline{v}'' + \alpha_1^4\underline{v} = i\alpha_1\bar{R}_{e_\delta}\left[(\bar{Q}_1 - \bar{C}_1)(\underline{v}'' - \alpha_1^2\underline{v}) - \bar{Q}_1''\underline{v}\right] \tag{3.13}$$

with the same boundary conditions on $\underline{v}$ as before, but with the boundary conditions $\bar{Q}_1(0) = 0$, $\bar{Q}_1(1) = 1.0$.

Thus, equation (3.13) is the Orr-Sommerfeld equation for the flat plate flow stability problem since $\bar{Q}_1 = f_o'$. It has been studied extensively and an approximate solution for the minimum critical Reynolds number, $\bar{R}_{e_I}$, based on displacement thickness can be written as

$$\bar{R}_{e_\delta} = \frac{43.1\left(\frac{\partial \bar{Q}_1}{\partial z}\right)_{wall}}{\bar{C}_1^4} \tag{3.14}$$

where $\bar{C}_1$ is the dimensionless wave speed determined by the condition for neutral stability:

$$\bar{Q}_1(\bar{C}_1) = .58 = \frac{-\pi\left(\frac{\partial \bar{Q}_1}{\partial \eta}\right)_{wall}\bar{C}_1\left(\frac{\partial^2 \bar{Q}_1}{\partial \eta^2}\right)_{\bar{Q}_1=\bar{C}_1}}{\left(\frac{\partial \bar{Q}_1}{\partial \eta}\right)_{\bar{Q}_1=\bar{C}_1}} \tag{3.15}$$

This equation has been solved numerically and yields a value of $\bar{C}_1 = .4136$, which gives a minimum critical Reynolds number based on displacement thickness $\bar{R}_{e_1} = 485$. However, inverting equation (3.12c) for the Reynolds number yields

$$R_{e_1}\Big|_{\substack{\text{minimum}\\\text{critical}}} = 485\left(\frac{1 + (\frac{\beta}{\gamma})^2}{1 - \frac{\beta}{\gamma}\frac{\omega R}{V_\infty}}\right) \tag{3.16}$$

This Reynolds number (based on displacement thickness) is minimized for the condition

$$\frac{\beta}{\gamma} = -\frac{\omega R}{V_\infty} \tag{3.17}$$

giving

$$R_{e_1}\Big|_{\substack{\text{minimum}\\\text{critical}}} = \frac{485}{\sqrt{1 + (\frac{\omega R}{V_\infty})^2}} \tag{3.18}$$

This equation is plotted in Figure 2 and indicates that the spin rate of the body is a large factor in determining the stability of the boundary layer flow. Although the Reynolds number is plotted to a value of $\omega R/V_\infty = 1$, the results will be questionable when the inverse reduced Rossby number, $1/\omega^*$, is not small.

In this case the ratio given by equation (3.17) yields the minimum value and implies that the disturbances most likely to be amplified first will propagate in the direction of the velocity vector $\vec{V_\infty i} + \vec{\omega R k}$

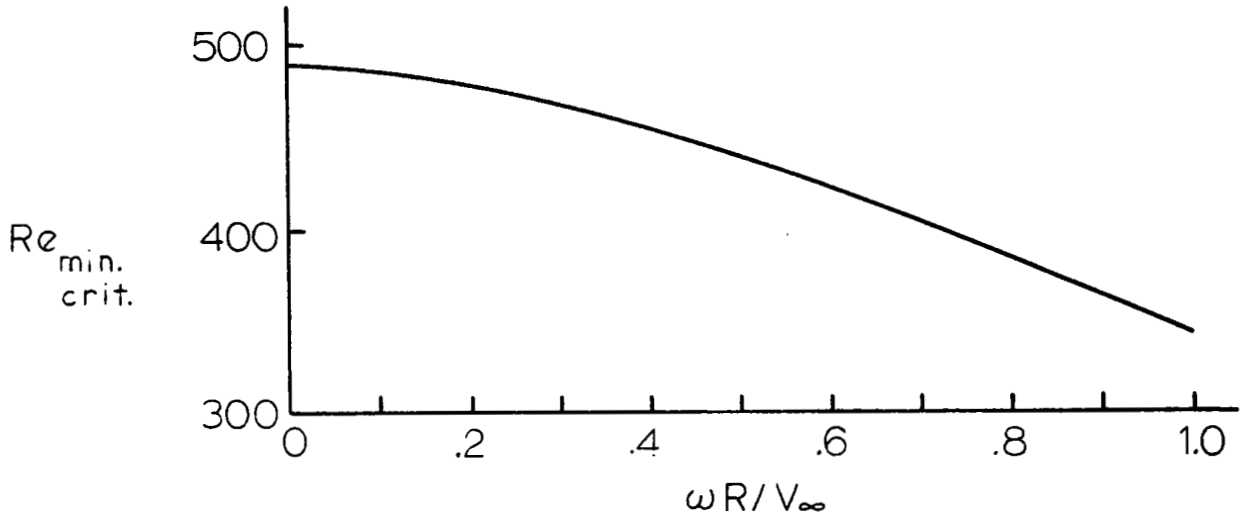

Figure 2 Minimum Critical Reynolds Number Based on Displacement Thickness Vs. $\frac{\omega R}{V_\infty}$

This is indeed the case indicated in Brown's photograph, and is consistent with what would be predicted by Squire's theorem.

3.3 Small Angles-of-Attack - Formulation

Now consider the case of small modified angle-of-attack, α_ℓ^*, which introduces significant complexity into the equations. The steady-state solution is written as

$$U = U_o + \alpha_\ell^* U_1 \tag{3.19a}$$

$$W = W_o + \alpha_\ell^* W_1 \tag{3.19b}$$

where

$$U_1 = 2V_\infty f_1(\eta)\cos\left(\frac{z}{R}\right) + \frac{V_\infty}{\omega_\ell^*} f_2(\eta)\sin\left(\frac{z}{R}\right) \tag{3.20a}$$

and

$$W_1 = 2V_\infty \frac{R}{L} f_0'(\eta)\sin\left(\frac{z}{R}\right) + \frac{V_\infty}{\omega_\ell^*}\frac{R}{L} h_0(\eta)\cos\left(\frac{z}{R}\right). \tag{3.20b}$$

As before, assume a disturbance given by equations (3.8) and substitute into equations (3.3) - (3.6). Neglecting terms $O(R_{e_L}^{-1/2})$ and letting

$$Q_1^* = \frac{U_o}{V} + \frac{\beta}{\gamma}\frac{W_o}{V} + \alpha_\ell^*\left(\frac{U_1}{V} + \frac{\beta}{\gamma}\frac{W_1}{V}\right); \text{ and, } \bar{C}_1 = \frac{c}{\gamma} \tag{3.21}$$

yields

$$\underline{v}'''' - 2\alpha_1^2\underline{v}'' + \alpha_1^4\underline{v} = iR_{e_\delta}\,\gamma[(Q_1^* - \bar{C}_1)(\underline{v}'' - \alpha_1^2\underline{v}) - Q_1^{*\prime\prime}\underline{v}] \quad (3.22)$$

The difference between this equation and that for the zero angle-of-attack case is the angle-of-attack and β/γ dependence of Q_1^*. In the limit of $\alpha_\ell^* \to 0$ this reduces to the equation as for the zero angle-of-attack case.

The boundary conditions are

$$\underline{v}(0) = \underline{v}'(0) = 0 \quad \underline{v}' \sim e^{-\alpha_1 \hat{y}} \quad \text{for} \quad \hat{y} \geq 1 \quad (3.23)$$

3.4 Numerical Solution

The function Q_1^* is not in general monotonic and for some values of $\frac{\beta}{\gamma}$ exhibits overshoot and/or inflection points (see Figure 3). Because of this, the analytic technique of Lin used in the zero angle-of-attack case does not necessarily apply. Intuition would suggest for small α^* and $1/\omega^*$ that the direction of propagation of the most unstable mode would be approximately given by $-\frac{\omega R}{V_\infty}$ and the height of the critical layer would not change much. If this is the case, then Lin's approximate technique should yield good results and would provide a rapid way of solving equation (3.22). However, as pointed out in the literature (e.g., Rosenhead[12]), inflection points can play an important and perhaps even dominant role in the stability question. In fact, Rosenhead suggests that the most unstable mode may be in the direction in which the inflection point corresponds to $Q_1^* = 0$, which in this case, would not be near $-\omega R/V_\infty$. The height of the critical layer would also be greatly changed so Lin's approximation would not be expected to work.

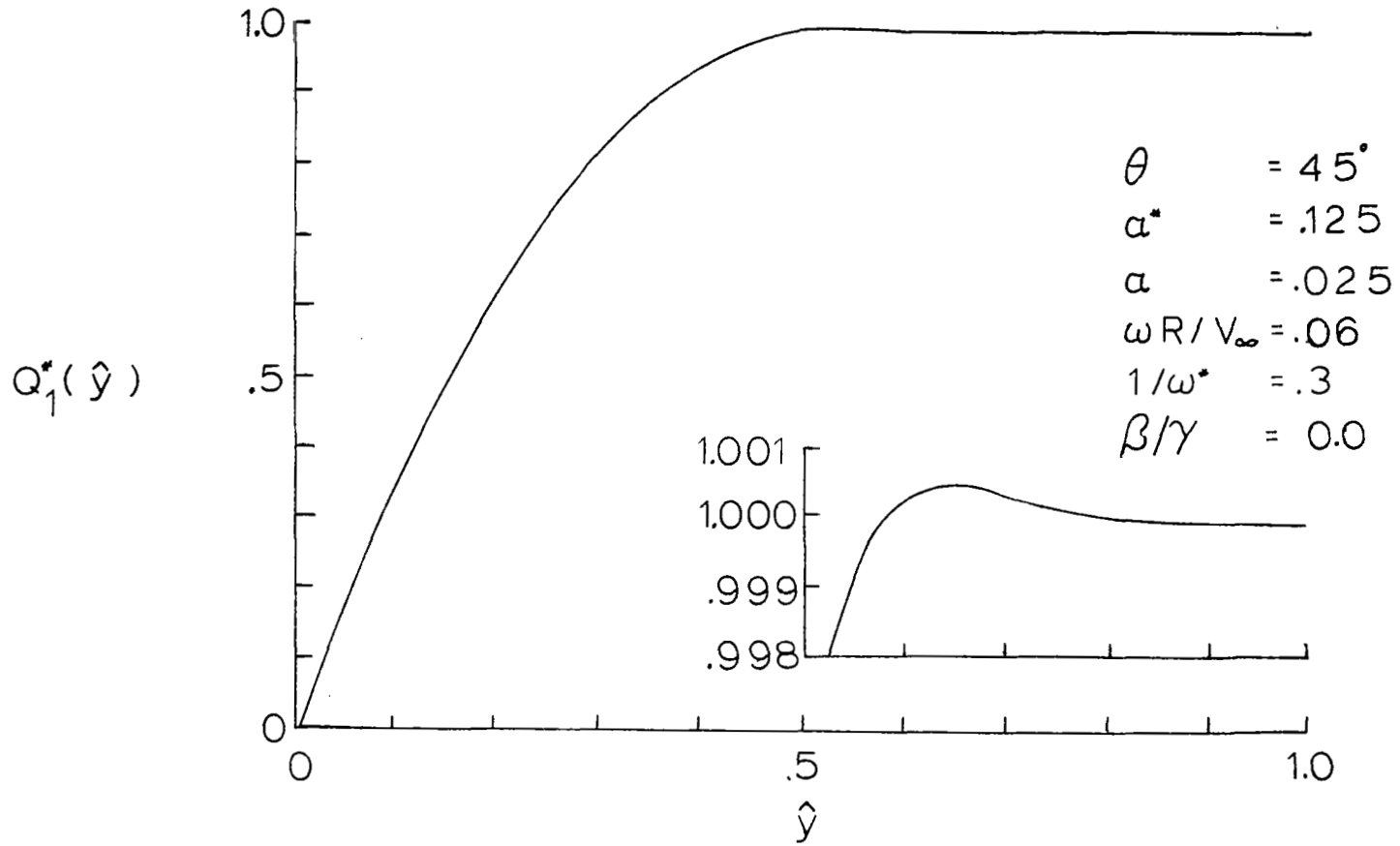

Figure 3 Boundary Layer Velocity Profile

To settle this question, equation (3.22) was solved numerically by a standard finite difference scheme for two point boundary value problems. The procedure consists of searching in α_1 and β/γ for the minimum critical Reynolds number at each azimuthal position. The results are shown in Figures 4 through 9 for typical values of the parameters.

Figures 4 and 5 indicate a marked variation in the minimum critical Reynolds number as a function of azimuthal angle. Included on these figures is the analytic solutions described in the next section. Figure 6 shows a typical neutral stability curve. There is considerable variation in the shape of the neutral stability curve depending on β/γ and azimuthal position.

The variation in the direction of propagation of the most unstable mode is indicated in Figure 7 for a typical case. It can be seen that the excursion from the $-\frac{\omega R}{V_\infty}$ direction is not substantial. This suggests that an approximate analytic solution with $\beta/\gamma = -\frac{\omega R}{V_\infty}$ should yield reasonable results since, as can be seen in Figure 8, the minimum critical Reynolds number variation near this value of β/γ is small. In addition the height of the critical layer, as indicated by the propagation velocity of the disturbance, $\bar{C}_{1R}$, does not vary substantially, cf Figure 9.

3.5 Approximate Solution

The results of section 3.4 indicate that an appropriate solution such as that of Lin should yield reasonable results. Introducing the transformations

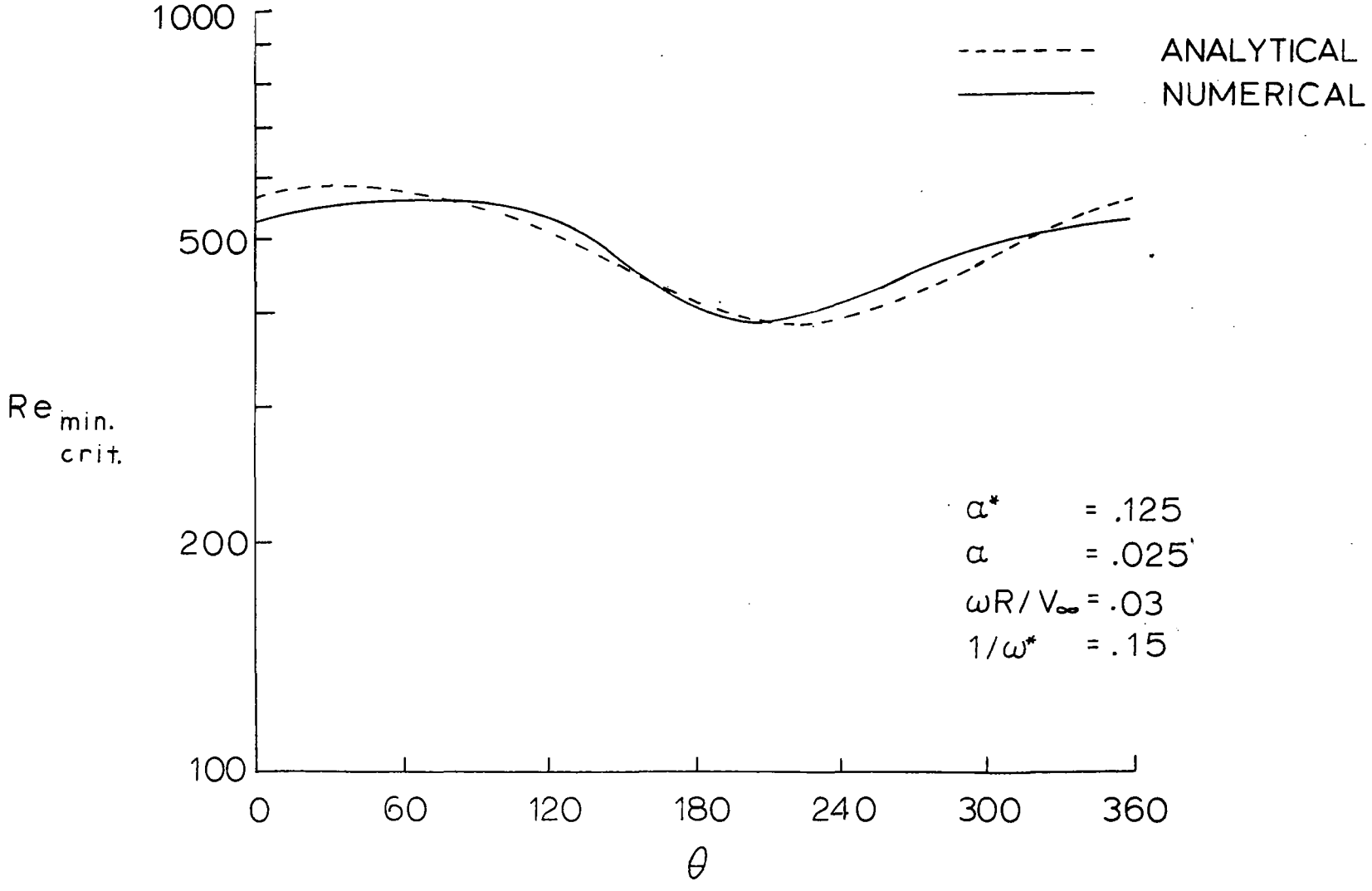

Figure 4 Minimum Critical Reynolds Number Based on Displacement Thickness Vs. θ
$\alpha^* = .125$, $1/\omega^* = .15$

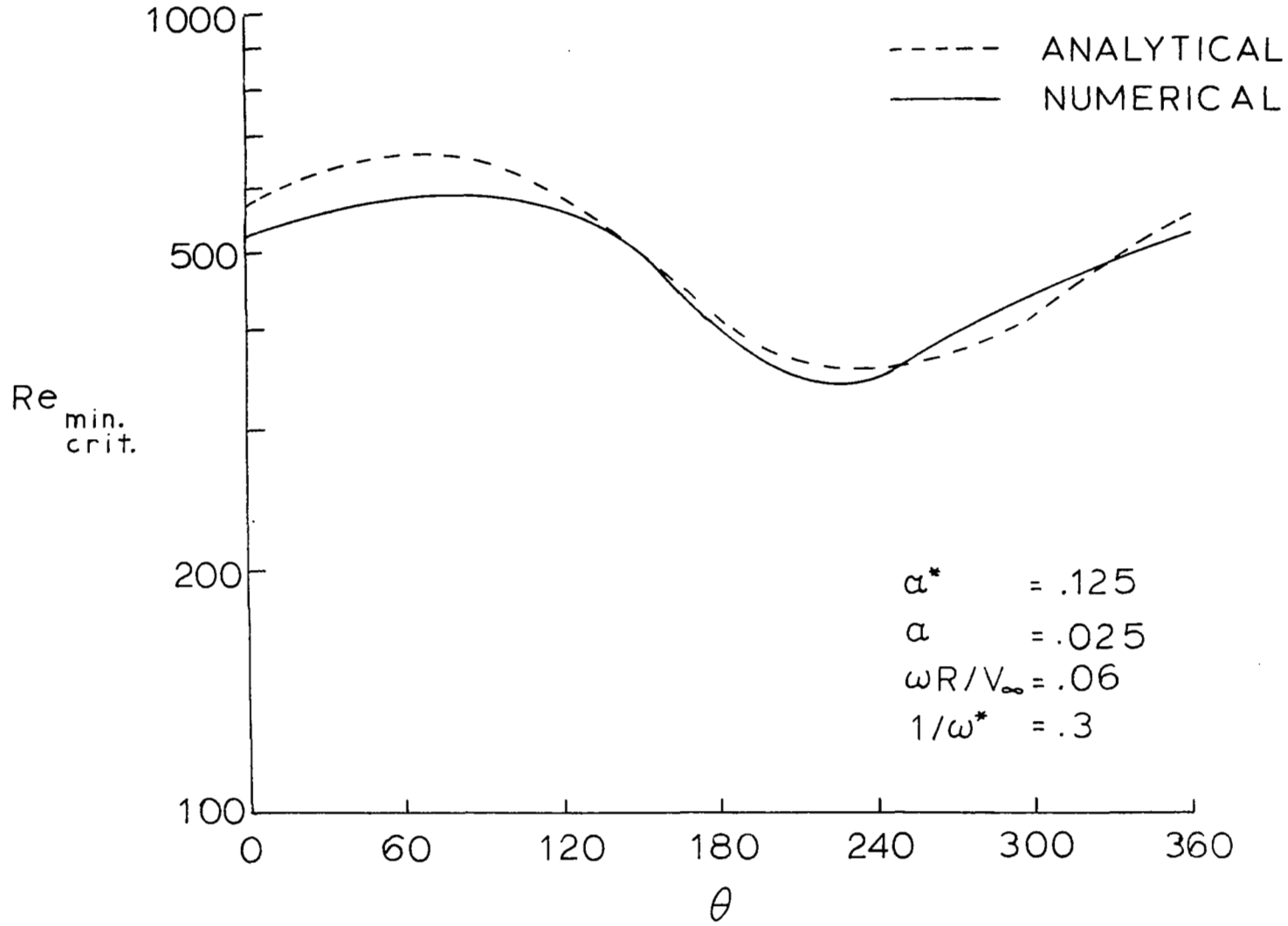

Figure 5 Minimum Critical Reynolds Number Based on Displacement Thickness Vs. θ
$\alpha^* = .125,\ 1/\omega^* = .3$

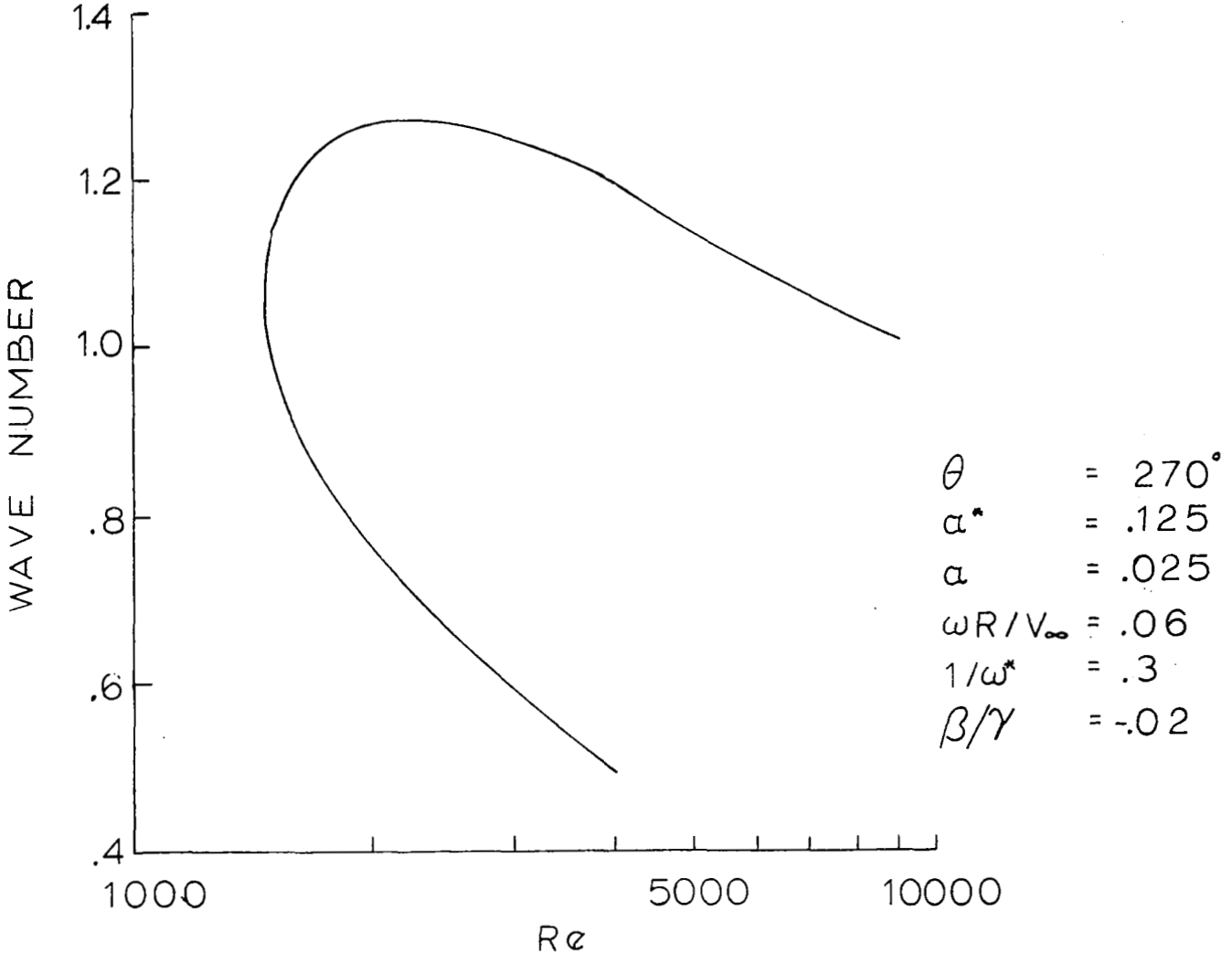

Figure 6 Neutral Stability Curve (Reynolds Number Based on Boundary Layer Thickness)

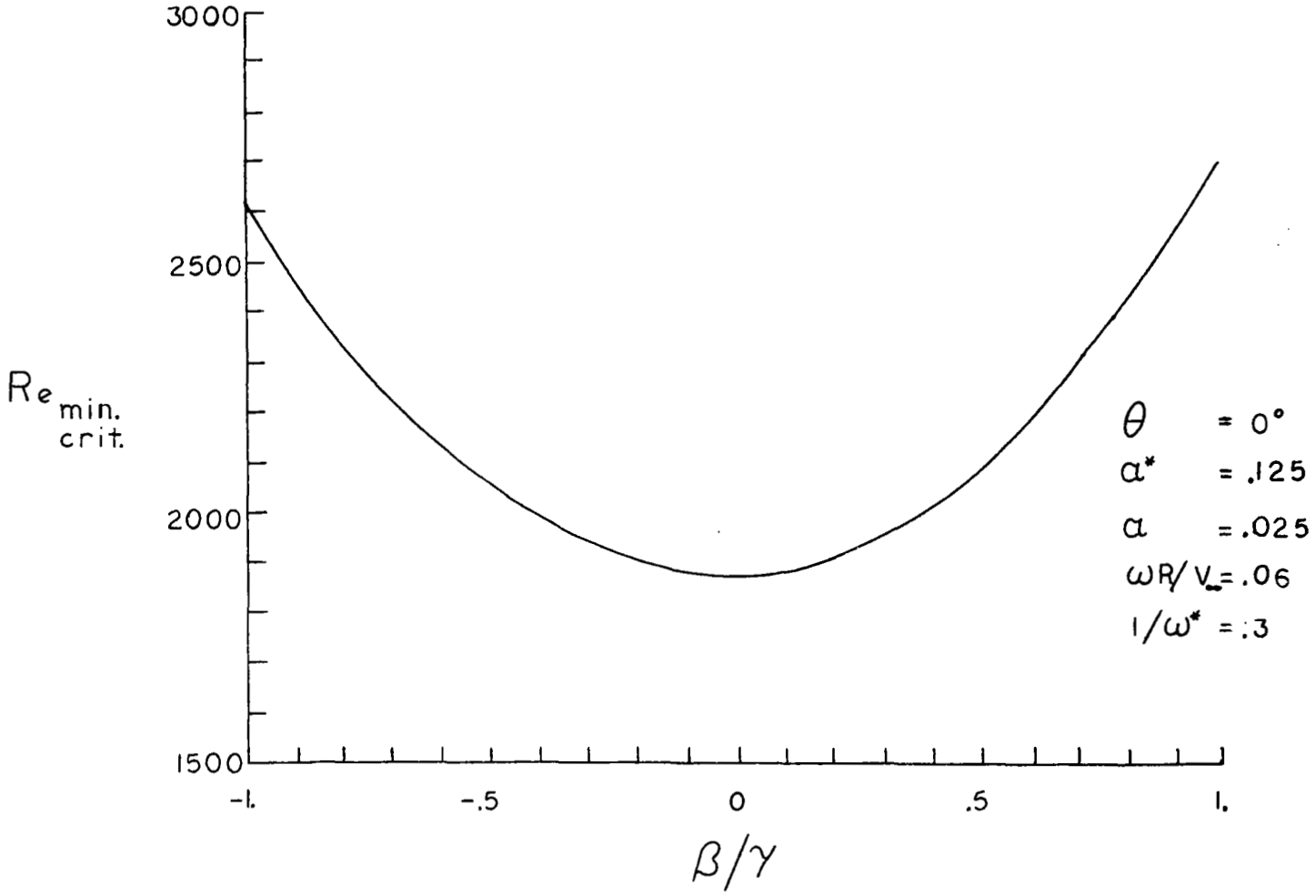

Figure 7 Minimum Critical Reynolds Number Vs. Variation in Direction of Propagation of Disturbance

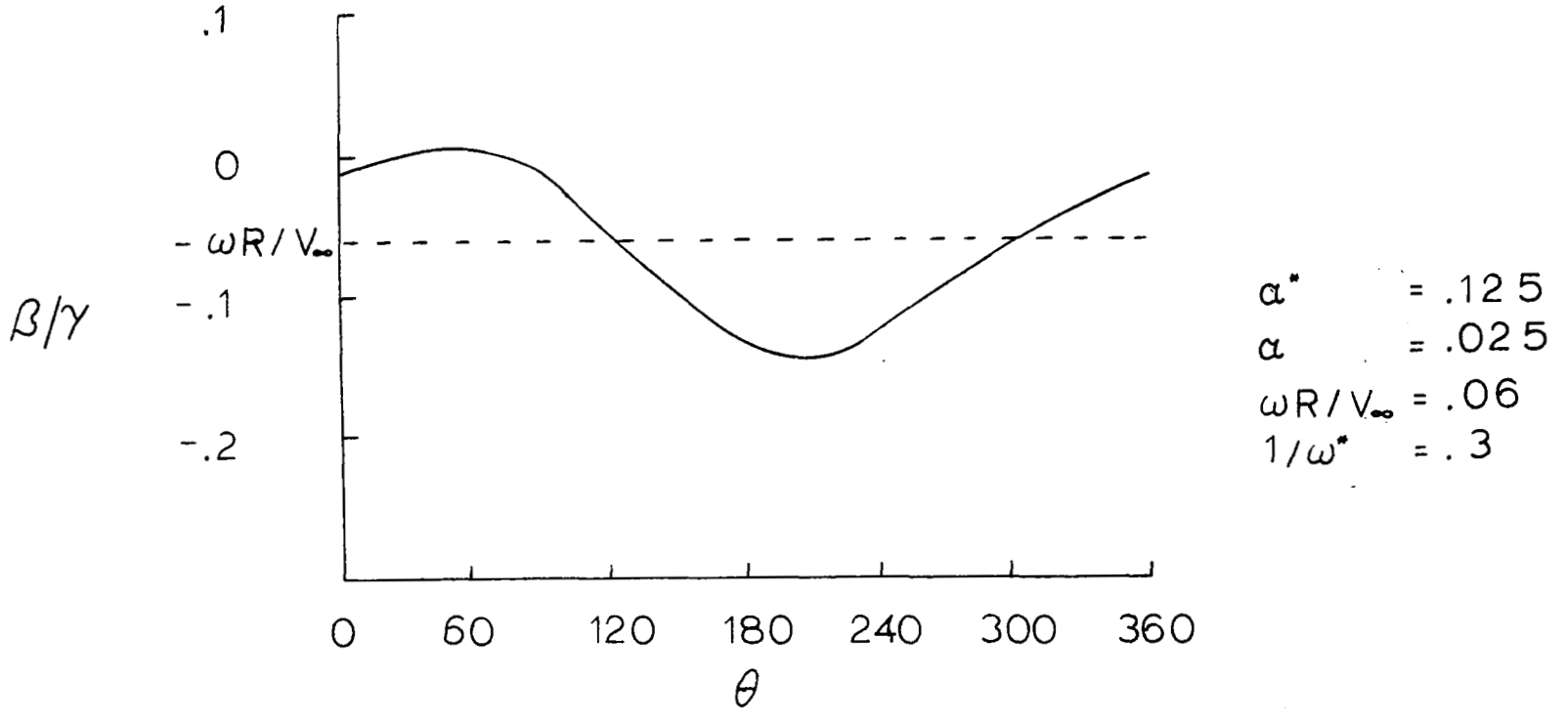

Figure 8 Effect of Azimuthal Position on Direction of Propagation of Most Unstable Mode

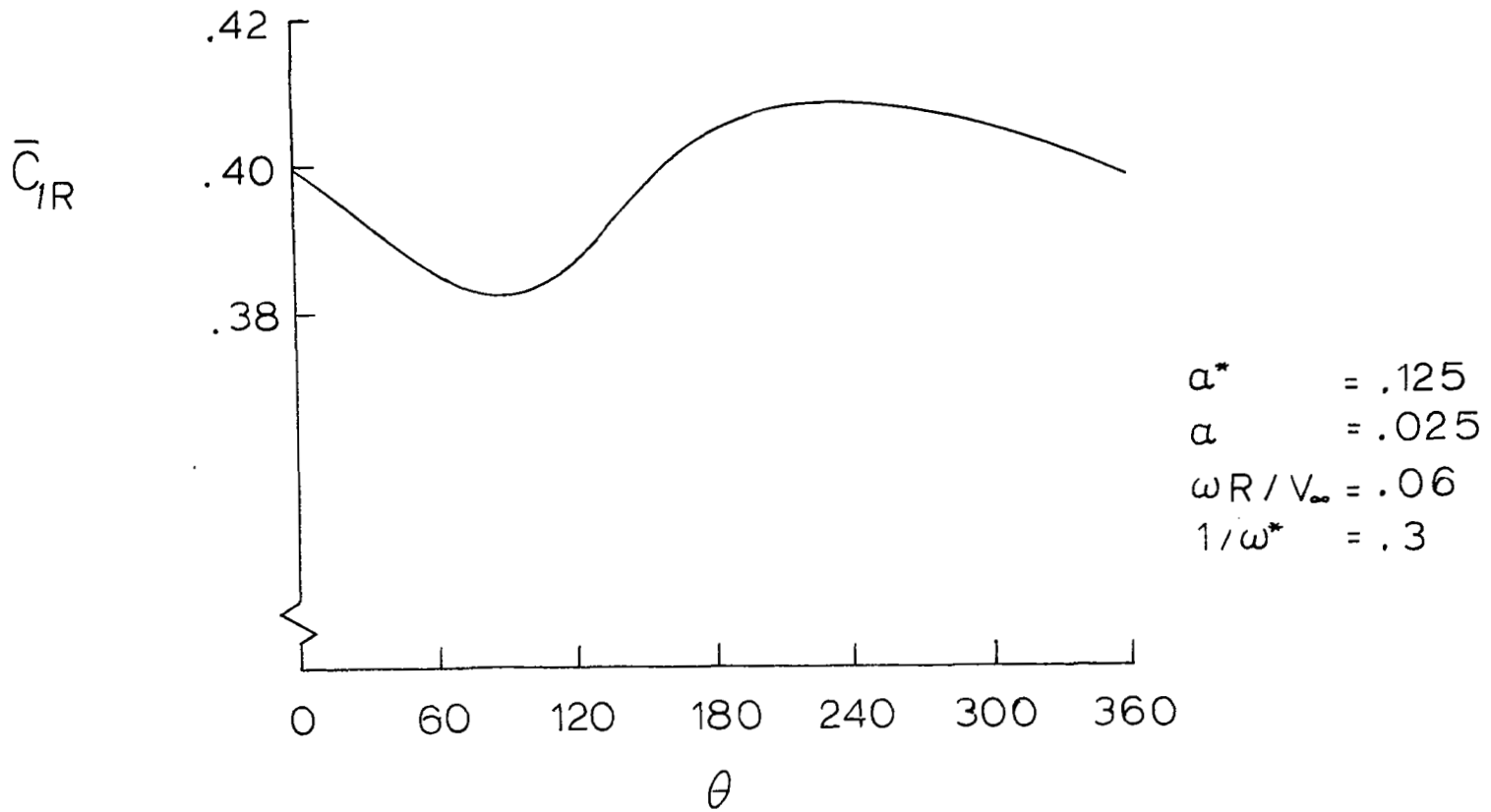

Figure 9 Wave Speed Vs. Azimuthal Position

$$\bar{Q}_1 = \frac{Q_1^* - \frac{\beta}{\gamma}\frac{\omega R}{V_\infty}}{1 + 2\alpha\frac{\beta}{\gamma}\sin\left(\frac{z}{R}\right) - \frac{\beta}{\gamma}\frac{\omega R}{V_\infty}} \tag{3.24a}$$

$$\bar{C}_1 = \frac{C_1 - \frac{\beta}{\gamma}\frac{\omega R}{V_\infty}}{1 + 2\alpha\frac{\beta}{\gamma}\sin\left(\frac{z}{R}\right) - \frac{\beta}{\gamma}\frac{\omega R}{V_\infty}} \tag{3.24b}$$

$$\bar{R}_{e_\delta} = \frac{\gamma}{\alpha_1}\left(1 + 2\alpha\frac{\beta}{\gamma}\sin\left(\frac{z}{R}\right) - \frac{\beta}{\gamma}\frac{\omega R}{V_\infty}\right)R_{e_\delta} \tag{3.24c}$$

and substituting into equation (3.22) gives

$$\underline{v}'''' - 2\alpha_1^2\underline{v}'' + \alpha_1^4\underline{v} = i\alpha_1\bar{R}_{e_\delta}\left[(\bar{Q}_1 - \bar{C}_1)(\underline{v}'' - \alpha_1^2\underline{v}) - \bar{Q}_1''\underline{v}\right] \tag{3.25}$$

with the same boundary conditions on v [equation (3.23)] but with $\bar{Q}_1(0) = 0$ and $\bar{Q}_1(1) = 1$. The solution for the approximate minimum critical Reynolds number is given by equation (3.14).

Due to the introduction of angle-of-attack, the solution is three dimensional in character, and a simple similarity solution no longer exists. That is, the steady-state solution no longer depends on $\hat{y}$ alone, but now depends on $\hat{x}$ and $\hat{z}$ as well. In equation (3.15) the calculation of the wave speed no longer can be accomplished independent of position on the body.

These equations are solved by assuming that the effect of a small angle-of-attack on the value of $\hat{y}$ for the critical height, and the associated wave speed $\bar{C}_1$ will be small, hence

$$\hat{y} = \hat{y}_o + \alpha_\ell^* y_1 \tag{3.26}$$

which yields the following expression for the wave speed[13]

$$\bar{C}_1 = \frac{[.4136 - .1307\alpha_\ell^* \ell(\hat{y}_o)][1 + (\frac{\omega R}{V_\infty})^2] + \alpha_\ell^* \varepsilon(\hat{y}_o)}{1 + (\frac{\omega R}{V_\infty})^2 - 2\alpha \frac{\omega R}{V_\infty} \sin(\frac{z}{R})} \tag{3.27}$$

where the functions ℓ, ε are given in reference 13, and $\hat{y}_o$ is the value of $\hat{y}$ corresponding to the zero angle-of-attack case. The minimum critical Reynolds number in this case can be written as

$$R_{e_{\delta}}\Big|_{\substack{\text{minimum}\\ \text{critical}}} = \frac{43.1}{\bar{C}_1^4} \sqrt{1 + (\frac{\omega R}{V_\infty})^2} \left\{ \frac{.3321[1 + (\frac{\omega R}{V_\infty})^2] + \alpha_\ell^* \varepsilon'(0)}{[1 + (\frac{\omega R}{V_\infty})^2 - 2\alpha \frac{\omega R}{V_\infty} \sin(\frac{z}{R})]^2} \right\} \tag{3.28}$$

As can be seen in Figures 4 and 5 this approximate solution yields gratifying results. In addition, Figure 10 illustrates the dependence of the minimum critical Reynolds number on the two parameters α^* and $1/\omega^*$. The introduction of an angle-of-attack makes the boundary layer more susceptible to the effects of spin. It should be noted here that for the larger values of α^* and $1/\omega^*$ this data should be considered only qualitative in nature due to the assumptions made.

Preliminary experimental results[13] indicate that the "transition line" is indeed skewed with respect to the plane of the angle-of-attack in the same general way as predicted by this analysis.

3.6 Magnus Effect

The "small disturbance" analysis suggests that the transition of the boundary from laminar to turbulent flow occurs asymmetrically which would

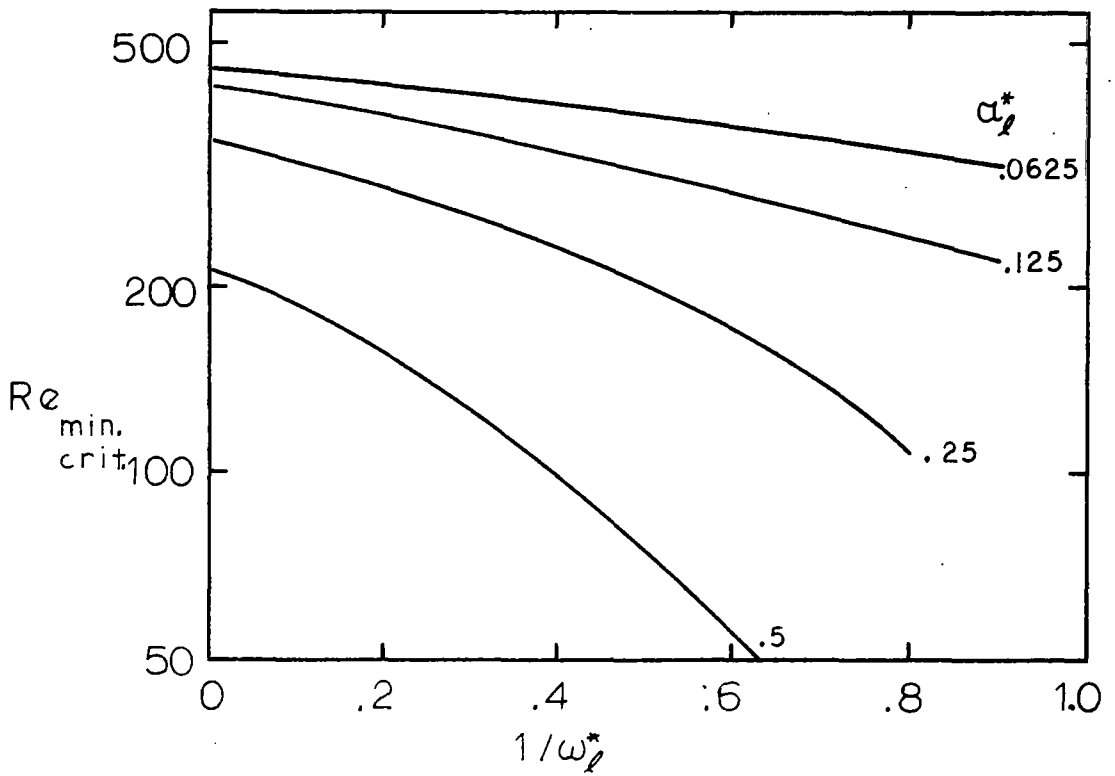

Figure 10 Minimum Critical Reynolds Number (Based on Displacement Thickness) Vs. α_ℓ^* and $1/\omega_\ell^*$

result in an asymmetric growth of the boundary layer (Figure 11). The The Magnus effect resulting from considering the potential flow about a "new" body, whose effective shape includes the displacement thickness, can be determined using slender body theory.

The velocity potential can be written as

$$\Phi = \Phi_i + \phi \tag{3.29}$$

where Φ_i is the inviscid potential solution and ϕ is the perturbation potential due to the boundary layer. Assuming $\frac{\partial^2\phi}{\partial x^2}$ is small, the perturbation potential must satisfy only Laplace's equation (in polar coordinates) at each station, x, with the boundary conditions

$$\left.\frac{\partial\phi}{\partial y}\right|_{y\to\omega} = 0 \qquad \left.\frac{\partial\phi}{\partial y}\right|_{y=0} = \text{outflow velocity} = V_\infty\frac{\partial\Delta}{\partial x} \tag{3.30a, b}$$

where Δ is the boundary layer displacement thickness and $\frac{\partial\Delta}{\partial x}$ is the slope of the effective body shape.

The boundary layer displacement thicknesses grow at different rates for laminar[10] and turbulent[13] flows. For the turbulent case the growth was assumed to follow that of a boundary layer on a flat plate. Although not entirely adequate it was felt that this was sufficient to give a qualitative indication of the effect of the skewed transition line.

The transition from laminar to turbulent flow is assumed to take place at a Reynolds number proportional to the minimum critical Reynolds number. This is not strictly correct since in actual practice the transition depends on many factors (e.g., free stream turbulence level, surface

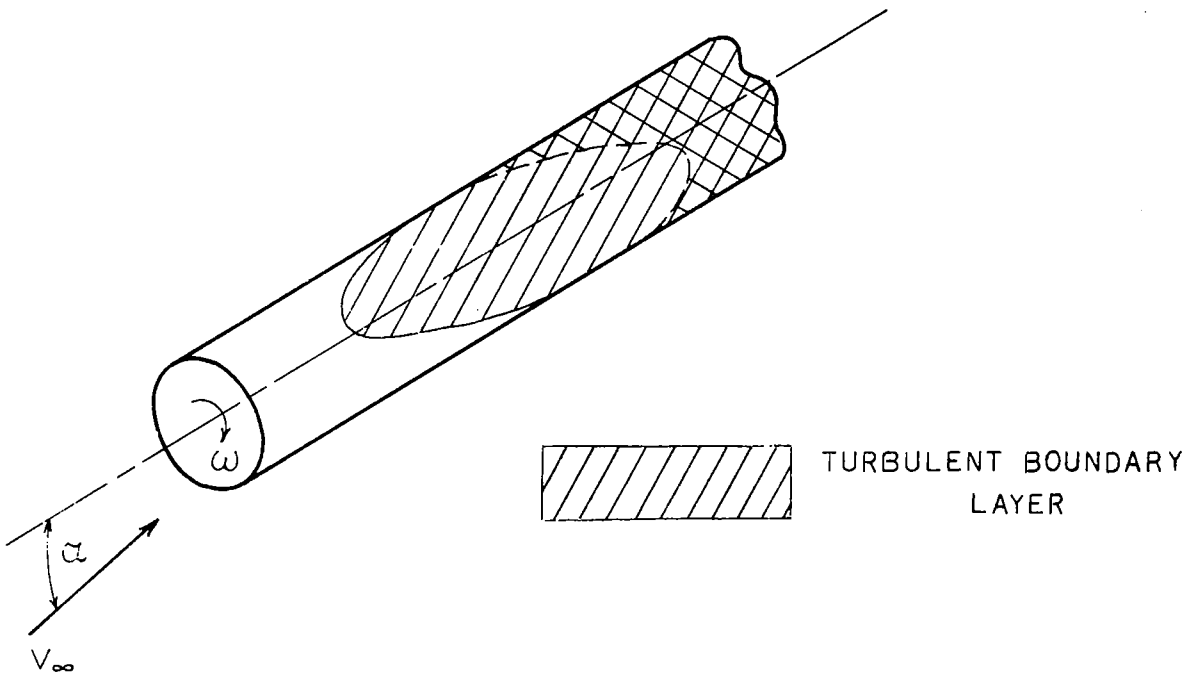

Figure 11 Asymmetric Boundary Layer

roughness, etc). However, this will tend only to shift the results in terms of Reynolds number without affecting the qualitative behavior, as will be seen below.

Laplace's equation with the above boundary conditions yields a solution for the perturbation potential which can be used to calculate the pressure coefficient. The pressure coefficient is given by

$$C_P = -\frac{2R}{\pi}\frac{\partial I}{\partial x}\sin\left(\frac{z}{R}\right) \tag{3.31}$$

where

$$I = \int_0^{2\pi} \frac{\partial \Delta}{\partial x}\sin\left(\frac{z}{R}\right)\, d\left(\frac{z}{R}\right) \tag{3.32}$$

Integrating the pressure coefficient to obtain the Magnus force and moment yields:

$$F_{mag} = -2R^2 q_\infty I(L) \tag{3.33}$$

$$M_{mag} = -2R^2 q_\infty \left[I(L)L - \int_0^{2\pi} \Delta(L)\sin\left(\frac{z}{R}\right)d\left(\frac{z}{R}\right)\right] \tag{3.34}$$

since the value of the integral I is zero at $x = 0$.

Integrating equations (3.33) and (3.34) (exactly) for the cases of fully laminar or fully turbulent boundary layer flow, yields the same results as Martin.[10] For the laminar case

$$F_{mag} = \frac{41.31}{\sqrt{\frac{V_\infty L}{\nu}}} q_\infty \alpha \frac{\omega R}{V_\infty} L^2 \qquad (3.35)$$

$$M_{mag} = \frac{24.78}{\sqrt{\frac{V_\infty L}{\nu}}} q_\infty \alpha \frac{\omega R}{V_\infty} L^2 \qquad (3.36)$$

and for the turbulent case

$$F_{mag} = \frac{1.237}{\sqrt[5]{\frac{V_\infty L}{\nu}}} q_\infty \alpha \frac{\omega R}{V_\infty} L^2 \qquad (3.37)$$

$$M_{mag} = \frac{.725}{\sqrt[5]{\frac{V_\infty L}{\nu}}} q_\infty \alpha \frac{\omega R}{V_\infty} L^2 \qquad (3.38)$$

For the more general case, the analysis is carried out numerically. The Magnus force is shown in Figure 12 for a range of Reynolds number a function of angle-of-attack calculated using equation (3.33). The Magnus force predicted with an asymmetric mixed boundary layer is somewhat greater than that predicted with Martin's theory.

The most striking result is in the behavior of the center of pressure of the Magnus force (Figure 13).

$$X_{CP} = \frac{M_{mag}}{F_{mag}} \qquad (3.39)$$

The center of pressure predicted on the bases of the asymmetric transition can be well forward of the fully laminar case. Due to the uncertainties in the parameters which determine the actual transition Reynolds number direct correlation with experimental data is not possible; the trends, however, agree quite well.[14,15]

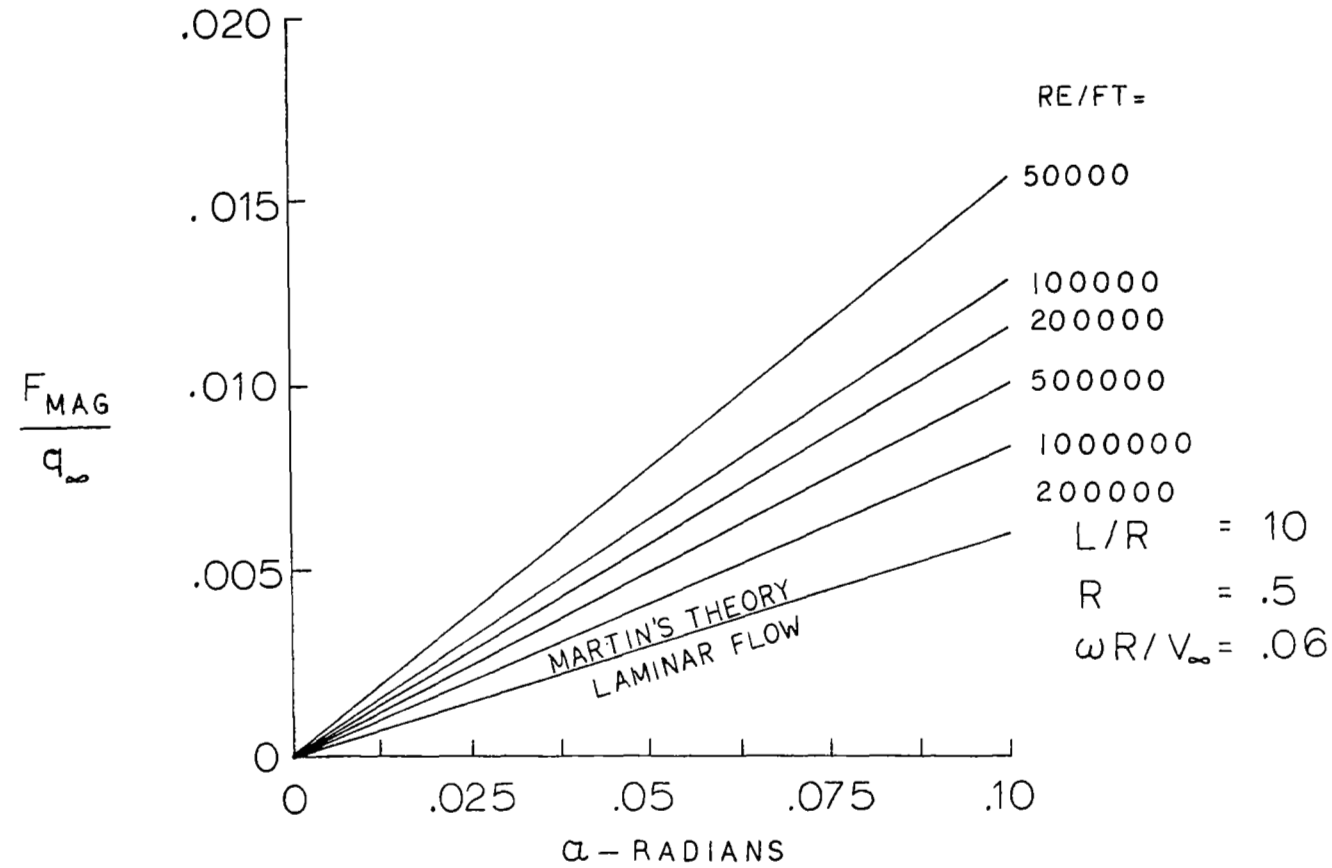

Figure 12 Magnus Force Vs. Angle-of-Attack

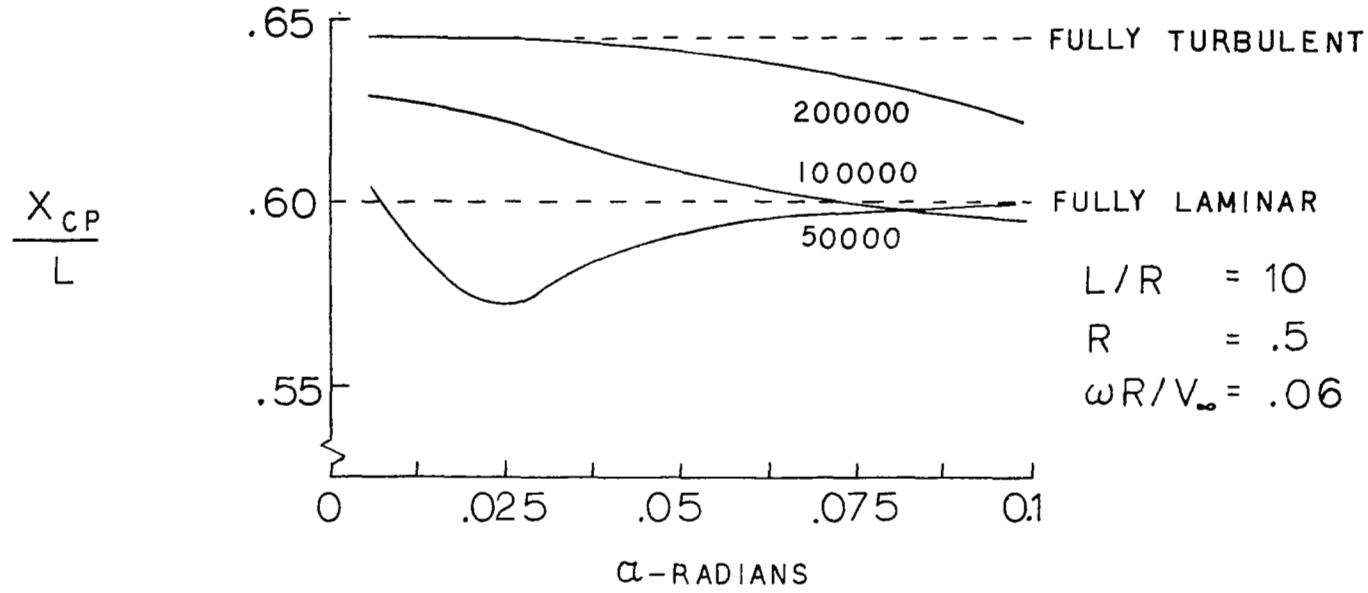

Figure 13 Magnus Center of Pressure Vs. Angle-of-Attack ($R_{e_{transition}}$ = 80,000)

These results can only be used as an indication of the effect Reynolds number variation has on the Magnus center of pressure. If the actual transition Reynolds number based on body length is, for example, 200,000 at zero spin and zero angle-of-attack (as opposed to the assumed 80,000 above), then the behavior of the center of pressure for a given free stream Reynolds number and angle-of-attack changes. A comparison can be seen in Figure 14, where the center of pressure location is plotted for an assumed transition Reynolds numbers of 200,000. A very similar behavior is observed as in the previous case - the primary difference being the magnitude of the free stream Reynolds number for each curve.

Acknowledgements: The authors wish to thank Mr. John Gary of the National Center for Atmospheric Research for making available the computer program used to solve the Orr-Sommerfeld equation. More details of this program are available in reference 16.

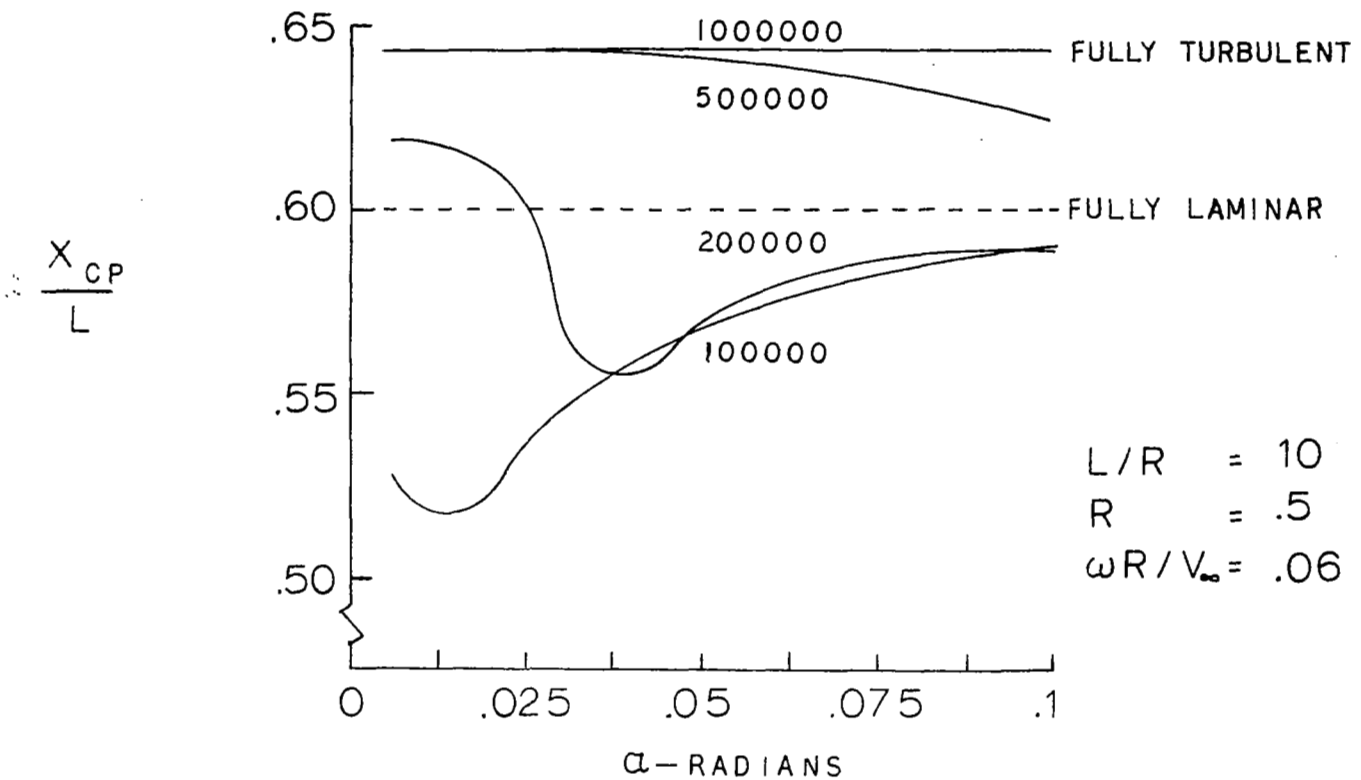

Figure 14 Magnus Center of Pressure Vs. Angle-of-Attack ($R_{e_{transition}}$ = 200,000)

REFERENCES

1. W. M. F. Orr, Proc. Roy. Irish Acad., 27, 1906-1907.

2. A. Sommerfeld, Proc. 4th Int. Congress Math., Rome, 1908.

3. W. Tollmein, Zeit. angew. Math. Mech., 15, 1935.

4. H. Schlichting, Boundary Layer Theory, 4th Edition, McGraw-Hill, New York, 1960.

5. Lin, "On the Stability of 2-D Parallel Flows, Parts I, II, III," Quart. of Applied Mathematics, Vol. 1-3, 1943-1946.

6. Squire, "On the Stability for 3-D Disturbances of Viscous Fluid Flow between Parallel Walls," Proc. of Royal Society of London, Series A, Vol. 142, 1933.

7. Kuethe, "Some Aspects of Boundary Layer Transition and Flow Separation on Cylinders in Yaw," First Midwestern Conference on Fluid Dynamics, Ann Arbor, Michigan, 1951.

8. Thorman, "Boundary Layer Measurements on an Axisymmetric Body with Spin and Yaw," California Institute of Technology, Ph.D. Thesis, 1958.

9. Furuya, Nakamura and Kawachi, "The Experiment on the Skewed Boundary Layer on a Rotating Cone," Bulletin of JSME, Vol. 9, No. 36, 1966.

10. J. C. Martin, "On Magnus Effects Caused by the Boundary Layer Displacement Thickness on Bodies of Revolution at Small Angles-of-Attack," Ballistic Research Laboratories, Report 870-Revised, June 1955. (A condensed version appeared in J. Aeronaut. Sci., 24, p. 421, 1957).

11. F. Brown, Proceedings of the Sixth Midwestern Conference Fluid Mechanics, 1953.

12. Rosenhead, L., Ed. Laminar Boundary Layers, Oxford University Press, 1963.

13. I. D. Jacobson, "Influence of Boundary-Layer Transition on the Magnus Effect", Ph.D. Dissertation, University of Virginia, June 1970.

14. S. A. Nikitin, "Aerodynamic Characteristics of a Spinning Body of Revolution Situated at an Angle-of-Attack in a Flow," Akademiia Nauk Latviiskoi SSR, Izvestiia, Seriia Fizicheskikh k Tekhnicheskikh Nauk, No. 6, pp. 63-70, 1967, In Russian.

15. T. R. Sieron, "On the 'Magnus Effects' of an Inclined Spinning Shell at Subsonic and Transonic Speeds," WADD TR60-212, 1961.

16. J. Gary and Helgason, "A Matrix Method for Ordinary Differential Eigenvalue Problems", J. of Comp. Phys. 5, pp. 169-187, 1970.